

Article

Comparison of Saturated and Superheated Steam Plants for Waste-Heat Recovery of Dual-Fuel Marine Engines

Marco Altosole ¹, Giovanni Benvenuto ^{2,*}, Raphael Zaccone ²  and Ugo Campora ³

¹ Dipartimento di Ingegneria Industriale (DII), School of Polytechnic and Basic Sciences, University of Naples “Federico II”, 80138 Naples, Italy; marco.altosole@unina.it

² Dipartimento di Ingegneria Navale, Elettrica, Elettronica e delle Telecomunicazioni (DITEN), University of Genoa, Via Montallegro 1, I-16145 Genova, Italy; raphael.zaccone@edu.unige.it

³ Dipartimento di Ingegneria Meccanica, Energetica, Gestionale, Trasporti (DIME), University of Genoa, Via Montallegro 1, I-16145 Genova, Italy; campora@unige.it

* Correspondence: giovanni.benvenuto@unige.it; Tel.: +39-348-665-3079

Received: 16 January 2020; Accepted: 18 February 2020; Published: 22 February 2020



Abstract: From the working data of a dual-fuel marine engine, in this paper, we optimized and compared two waste-heat-recovery single-pressure steam plants—the first characterized by a saturated-steam Rankine cycle, the other by a superheated-steam cycle—using suitably developed simulation models. The objective was to improve the recovered heat from the considered engine, running with both heavy fuel oil and natural gas. The comparison was carried out on the basis of energetic and exergetic considerations, concerning various aspects such as the thermodynamic performance of the heat-recovery steam generator and the efficiency of the Rankine cycle and of the combined dual-fuel-engine–waste-heat-recovery plant. Other important issues were also considered in the comparison, particularly the dimensions and weights of the steam generator as a whole and of its components (economizer, evaporator, superheater) in relation to the exchanged thermal powers. We present the comparison results for different engine working conditions and fuel typology (heavy fuel oil or natural gas).

Keywords: heat-recovery systems; marine propulsion plants; combined-cycle power plants; emission reduction

1. Introduction

Currently, most engines used for ship propulsion still consist of diesel engines fueled by traditional fuel types, such as Heavy Fuel Oil (HFO) and Marine Diesel Oil (MDO). However, in recent years, there has been an increasingly widespread use of Dual-Fuel (DF) engines capable of burning both diesel fuels and natural gas (NG), motivated by a series of technical and environmental advantages. The growing demand for a reduction in the polluting emissions of ships, promoted by increasingly restrictive international regulations, has in fact favored interest in engines powered by natural gas that could significantly reduce emissions of sulfur oxides, nitrogen oxides, particulate matter, and carbon dioxide [1]. Regulations adopted by the International Maritime Organization (IMO), initially focused on sulfur and nitrogen oxides [2], were subsequently oriented toward carbon dioxide emissions [3,4] due to the need of reducing the greenhouse effect. The reduction of CO₂ emissions can be achieved by using fuels characterized by low carbon content, such as natural gas [5], but also by improving the efficiency of marine propulsion systems, with positive effects on the reduction of fuel costs. An example of a typical reduction of pollutant emissions of an NG-fueled engine in comparison with a diesel engine fueled with HFO was reported in [6]: 25 ÷ 30% carbon dioxide, 25% carbon monoxide,

85% NO_x, 98 ÷ 100% SO_x, 98 ÷ 99% particulate matter. With regard to the other aspect mentioned above, namely the efficiency improvement of ship propulsion plants, with positive implications on emissions and fuel costs, many solutions have recently been proposed, including those that are based on the recovery of heat contained in the exhaust gases of the main engine by means of Waste Heat Recovery (WHR) systems. Among these solutions we can mention turbocharging [7,8], turbocompounding [9], thermochemical recuperation [10], thermoelectrics [11], cabin cooling [12], and of course WHR steam plants [13]. The adoption of this last solution, of particular interest in the marine propulsion sector, allows to satisfy the vessel heat necessity and, at the same time, to produce electric energy by means of a steam turbine, then reducing the power of on-board diesel generators and their emissions. It should also be noted that the use of steam plants in WHR systems is not limited to diesel engines. In [13], possible applications were examined in ships using gas turbines as a prime mover, where the possibility of exploiting part of the thermal energy of exhaust gases by means of a steam plant, thus generating a Combined Gas and Steam (COGAS) system, makes it possible to increase the efficiency of the propulsion system and limit polluting emissions. More generally, with regard to the use of steam plants in recent and current applications to marine propulsion, the case of commercial Liquefied Natural Gas (LNG) carriers is particularly significant. The choice of propulsion system for this type of ship depends on the type of transported cargo, i.e., liquefied natural gas at a temperature of approximately −160 °C, below its boiling point at the corresponding pressure inside the tanks. Despite the thermal insulation of the tanks, designed to minimize heat supply from the outside, even a small part of this heat causes partial evaporation of the load, known as boil-off-gas (BOG). Depending on the modality of using the BOG and the type of power transmission (mechanical or electric drive), it is possible to identify main propulsion solutions for LNG carriers. In the case of BOG used as fuel, the solution adopted since the 1960s is that of a steam turbine with mechanical drive. This solution is still the most common on the market today [14], with a percentage of the LNG fleet above 40% (44% in May 2017). However, since 2004, several other solutions have been proposed with the use of both gas turbines and diesel engines. Among these are DF gas turbines with an electric drive, Combined Gas turbines and Electric Steam turbines (COGES), DF medium-speed diesel engines with an electric drive, and DF low-speed diesel engines with a mechanical drive. In the case of recovered BOG, the most considered solution by the market after 2010 [14] is that of the single-fuel, two-stroke, low-speed engine with a mechanical drive and a re-liquefaction plant, which has currently reached a percentage of the LNG fleet of about 40% (41% in May 2017). More details on propulsion systems for LNG carriers and their evaluation can be found in [14,15].

2. WHR Steam Plants Overview

Many examples of WHR systems from marine diesel engines were presented in the literature, some of which are mentioned in references at the end of this paper [16–28]. Of the last two papers [27,28], the former is on the effects of the deterioration of steam-plant components on the performance of WHR systems, and the latter presents an interesting comparison of an organic and a steam Rankine cycle applied to WHR plants. To the authors' knowledge, only [6,26] refer to DF marine engines combined with WHR steam plants. All cited papers refer to single- and/or dual-pressure WHR superheated steam plants, with the only exception of [26], where a single-pressure saturated steam plant was used for waste-heat recovery of the main engine. In a previous paper of the authors [29], six WHR plants of different types (single- or dual-pressure, saturated- or superheated-steam) were optimized and compared for application to the propulsion engines of an existing cruise ferry. We found that, mainly in the case of single-pressure WHR steam plants, there was no substantial difference between the state of used steam (saturated or overheated) with regard to the power of the steam turbine and the efficiency of the Combined Engine–WHR system.

The main objective of this article is to demonstrate that the prevailing opinion from bibliographic analysis, which considers the use of the superheater in WHR systems convenient, has no scientific basis. For this reason, we wanted to contribute to clarify this issue by using a simulation methodology of these systems previously developed and validated. Following this observation, we carried out a thorough comparison between two single-pressure WHR plants, one characterized by saturated steam, the other by superheated steam, applied to the same DF four-stroke marine engine. Both WHR steam plants, characterized by a similar layout, were optimized by means of a simulation code, with a procedure presented by the authors in [24], aimed at achieving the best efficiency of the combined engine–WHR system with the engine running at Normal Continuous Rating (NCR). The WHR steam plants were then compared on the basis of energetic and exergetic considerations, with regard to the thermodynamic performance of the Heat Recovery Steam Generator (HRSG), the dimensions and weights of the steam generator as a whole and of its components (economizer, evaporator and superheater) in relation to the exchanged thermal powers, the Rankine cycle characteristics, and the efficiency of the combined DF engine–WHR plant.

The obtained results from the comparison for different engine working conditions and fuel type (HFO or NG) are then discussed and presented.

3. Case Study

In order to define the schemes of the WHR steam plants to be compared, it is necessary to know the characteristics of the propulsion engine to which these plants are applied and the electric- and thermal-power needs of the considered vessel.

The vessel in question is an existing cruise ferry of the GNV shipping line (overall length = 211 m; displacement = 49,257 tons; cruising speed = 22 knots). The propulsion system consisted of two controllable pitch propellers, each driven by two Wärtsilä 16V46C four-stroke diesel engines, of which the Maximum Continuous Rating (MCR) power is 16,800 kW at 500 rpm. In normal sea going conditions, only one of the two engines for each propeller shaft is active, and runs at Normal Continuous Rating (NCR), about 76% of the MCR. Electric users of the cruise ferry are powered by four Wärtsilä 6R32LNE diesel generators (2430 kWe at 720 rpm). The required thermal power by the Ship Steam Services (SSS) is satisfied by 1.15 kg/s of saturated steam at a pressure of at least 7 bar. On the basis of the shipowner indications, we considered that only part of the steam produced by a single WHR steam plant (one for each engine) was used to satisfy the thermal-power demand of the ship, while the remaining part was sent to a steam turbine for the production of electric energy.

In the simulation, the originally adopted diesel engine was substituted by a MAN 51/60 18V DF four-stroke engine, built by Man Diesel & Turbo, characterized by 17,550 kW of MCR power at 500 rpm [30]. A comparison of the main data of the two engines is shown in Table 1.

The choice of the new engine was motivated by the greater power and efficiency of the selected engine, as well as by more complete information availability.

To satisfy the ship's normal seagoing propulsion power and half the required SSS thermal power (0.57 kg/s), this new engine works at 488 rpm and at 75% MCR load, corresponding to 13,162.5 kW (NCR). When the engine is powered by natural gas (NG), the HFO fuel-tank heating is not necessary; consequently, ship SSS thermal power is reduced by 70% (only 0.17 kg/s of saturated steam for each running engine, at a pressure of at least 2 bar, sufficient in this condition).

The manufacturer data of the new DF engine [30], reported in Figure 1, show the remarkable difference in (a) exhaust-gas temperature, (b) mass-flow rate, and (c) thermal power between the two possible engine fuels (HFO or NG).

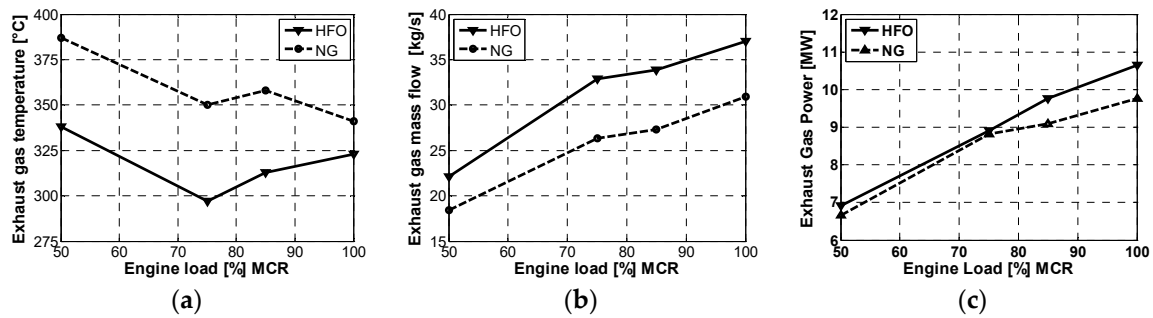


Figure 1. (a) Engine exhaust gas temperature, (b) mass-flow rate, and (c) thermal power versus engine load for two possible engine fuels.

Table 1. Comparison of main data of current and new engine.

Engine Parameters	Current Engine	New Engine
	Wärtsilä 16V 46C	MAN 51/60 18V DF
Length (mm)	12,871	13,644
Height (mm)	5854	5517
Width (mm)	4678	4713
Dry weight (tons)	233	265
Cylinders number	16	18
Bore (mm)	460	510
Stroke (mm)	580	600
Fuel type	HFO	HFO/NG
MCR power (kW) at 500 rpm	16,800	17,550
B.m.e.p. (bar)	26.14	19.09
Injection type	single	double
Efficiency (%)	45.97	47.68 (NG)

4. Schemes of the Selected WHR Steam Plants

In this section, the two considered WHR steam plants, applied to the above-mentioned MAN dual-fuel engine, are briefly described, with reference to the schemes shown in Figures 2 and 3.

The first was a single-pressure saturated-steam plant, of which the scheme is shown in Figure 2, also considered in a previous paper of the authors [26]. This WHR steam plant is basically composed of an HRSG comprising an economizer (E) and an evaporator (EV) that feeds a steam turbine (ST) to drive an electric generator (EG).

The turbine exhaust steam is condensed in a condenser (SCO), from which it is extracted by a condensing pump (SCP) and preheated in the Jacket Water (JW) heat exchanger before being sent to the Heat Water Tank (HWT), from which it is taken by the main feed pump (MFP).

After being warmed by the hot air leaving the turbocharger compressor in the scavenge air preheater (SC), the water is sent to the HRSG economizer (E). To satisfy SSS, part of the saturated steam is taken from the HRSG steam drum (SD), as shown in Figure 2.

The second WHR plant is a single-pressure superheated-steam plant, of which the scheme is shown in Figure 3.

The basic layout of the superheated-steam system was the same as that adopted by the saturated-steam system, but with the addition of a superheater (SH in Figure 3) in the HRSG that takes saturated steam from the SD and feeds the steam turbine with superheated steam.

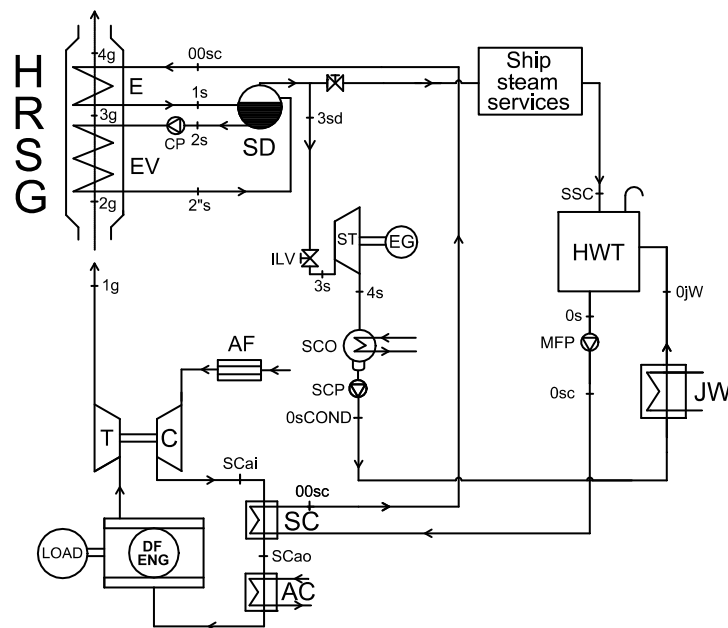


Figure 2. Waste-heat-recovery (WHR) single-pressure saturated-steam plant ($T_{1g} = T_{2g}$). *Abbreviations;* AC: aftercooler; AF: air filter; C: turbocharger compressor; CP: evaporator circulating pump; DF ENG: dual fuel engine; E: economizer; EG: electric generator; EV: evaporator; HWT: heat water tank; ILV: isenthalpic lamination valve; JW: jacket water; MFP: main feed pump; SC: scavenging system; SCai: scavenging air inlet; SCao: scavenging air outlet; SCO: steam condenser; SCP: steam cond. pump; SD: steam drum; SSC: ship steam services condenses; ST: steam turbine; T: turbocharger turbine; 1g: HRSG gas inlet; 2g: evaporator gas inlet; 3g: evaporator gas outlet; 4g: HRSG gas outlet; 0JW: jacket water outlet; 0s: heat water tank outlet; 0sc: main feed pump outlet; 0sCOND: steam cond. pump outlet; 00sc: scavenger water outlet; 1s: economizer outlet; 2s: evaporator circ. pump inlet; 2"s: evaporator outlet; 3s: steam turbine inlet; 3sd: SD saturated steam outlet; 4s: steam turbine outlet.

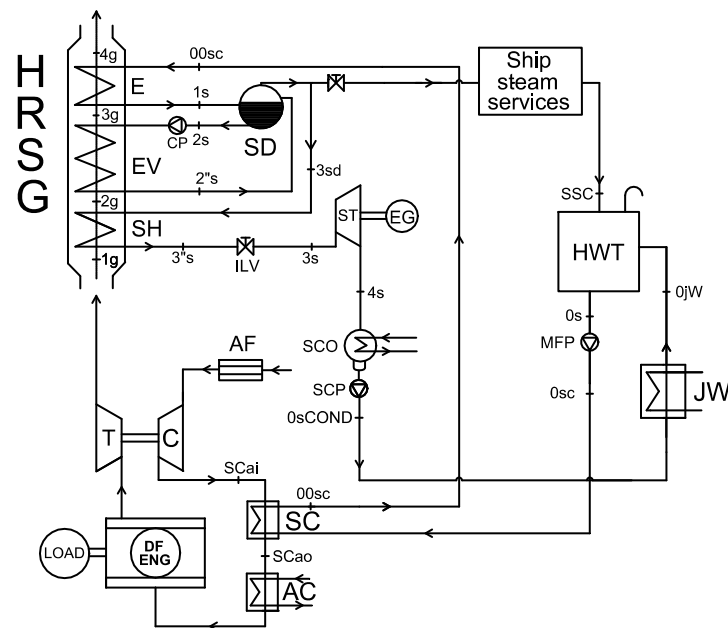


Figure 3. WHR single-pressure superheated-steam plant. *Abbreviations;* the same of Figure 2 with additions; SH: superheater; 1g: superheater gas inlet; 3"s: superheater steam outlet.

5. WHR Steam-Plant Simulation Models

In order to define the design characteristics of the selected WHR steam plants and evaluate their performance, we used two computer codes that we developed in MATLAB[®], as reported in [24].

The first code is able to calculate the dimensions, weight, and performance of the steam-plant components (HRSG economizer, evaporator, superheater, steam drum, steam turbine, hot well tank, etc.) in design working conditions, starting from available data of the DF engine (such as mass-flow rate and temperature of exhaust gas and scavenge air). The second code is used for the performance simulation of the WHR system (and relative components) in off-design working conditions.

Starting from the first code, the WHR steam-plant design procedure was based on steady-state continuity and energy equations:

$$\sum (M_i - M_o) = 0 \quad (1)$$

$$\sum (M_i h_i - M_o h_o) = Q' - P \quad (2)$$

where M_i and M_o are the fluid-mass-flow rates at the plant components' inlet and outlet sections, respectively; h the fluid-specific enthalpy; and Q' and P the heat and mechanical power exchanged with the outside, respectively. The heat exchangers of the considered HRSG were characterized by cross-counter flow configuration with horizontal finned tubes.

The overall heat-exchange coefficient (k_e) of the pipe wall for the various HRSG components was calculated as follows:

$$\frac{1}{k_e} = \frac{1}{h_e} + R_e + \frac{s}{k} \frac{A_e}{A_{ml}} + R_i \frac{A_e}{A_i} + \frac{1}{h_i} \frac{A_e}{A_i} \quad (3)$$

In this equation, h_e and h_i are external and internal pipe-convective heat-transfer coefficients; R_e and R_i are external and internal pipe thermal resistance; s and k are pipe-wall thickness and wall thermal conductivity, respectively; and A_e , A_i , and A_{ml} are pipe wall external, internal, and logarithmic area, respectively. Convective heat-transfer coefficients h_e and h_i were determined by using finned tube correlations [24]. For each HRSG heat exchanger, the total heat-exchange area (necessary for the pipe length evaluation) was calculated by means of heat-exchange balance equation:

$$Q'_g = k_g A_e (\Delta T)_{g-w} \quad (4)$$

which was relative to the gas-wall heat exchange, and:

$$Q'_s = k_s A_i (\Delta T)_{w-s} \quad (5)$$

which was relative to the wall-steam heat exchange.

In Equations (4) and (5), terms ΔT_{g-w} and ΔT_{w-s} , representing fluid-pipe-wall logarithmic temperature differences, are given, respectively, by:

$$(\Delta T)_{w-s} = \frac{T_{o-s} - T_{i-s}}{\ln\left(\frac{T_w - T_{i-s}}{T_w - T_{o-s}}\right)} \quad (6)$$

and:

$$(\Delta T)_{g-w} = \frac{T_{o-s} - T_{i-s}}{\ln\left(\frac{T_{i-g} - T_w}{T_{o-g} - T_w}\right)} \quad (7)$$

A similar procedure was used for the design of other heat exchangers of the steam plant: condenser (SCO), jacket water (JW), and scavenge air preheater (SC).

The steam-turbine simulation model was based on typical steady-state nondimensional mass-flow maps [31]. The efficiency of the steam turbine was evaluated by a correlation that took into account steam quality, as suggested by a steam-turbine manufacturer (Fincantieri S.p.A.). The HRSG steam

drum (SD) and hot well tank (HWT) were modelled as simple fluid-mixing tanks. The engine back-pressure value due to the HRSG was determined as reported in [24].

As mentioned before, a second computer code was developed to determine WHR steam-plant performance at both design and off-design steady-state load conditions. Starting from the design data of the plant components (geometric and functional characteristics), this second simulation code determined the WHR plant performance by using a calculation procedure reversed in some way with respect to the design one, as explained in [24].

WHR steam-plant design and off-design simulation procedures were validated in other papers by the authors [24,29] by comparing simulation results with existing corresponding experiment data. The comparison between calculated parameters and reference data was generally good for WHR steam plants operating under both design conditions (differences generally no more than 1%) and off-design conditions (differences generally less than 4%).

As an example of the validity of the presented simulation procedures, Table 2 shows a comparison taken from [24] that shows differences in terms of percentage errors between simulation results and experiment data concerning a dual-pressure WHR plant operating in design conditions, applied to a specific propulsion system consisting of a MAN two-stroke DE (6S70ME-C8.2), selected as prime mover of a 158,000 DWT crude-oil tanker (Suezmax), belonging to the Premuda company.

Table 2. Accuracy of developed design procedure [23].

Design-Code Results	% Error
HP _{Ti} : turbine inlet high pressure	0.01
LP _{Ti} : turbine inlet low pressure	0.00
M _{SHP} : turbine inlet steam mass-flow rate	0.05
M _{S LP} : turbine inlet steam mass-flow rate	0.52
T _{outG} : HRSG outlet gas temperature	0.54
P _{ST} : steam turbine power	0.75

6. WHR Steam-Plant Optimization

The adopted optimization model, based on the calculation procedures described above, is similar to that described in [24]. In this study, the optimization procedure starts from the consideration that DF engines predominantly work powered by NG, and only occasionally use diesel fuel [26].

Therefore, performance optimization of the Dual Fuel engine–WHR Combined Plant (DF–WHR CP) had to consider the engine powered by NG.

Once defined the WHR steam-plant layouts (see Figures 2 and 3), the operative engine NCR (488 rpm and 13,162.5 KW), and the SSS steam mass-flow rate, the Rankine cycle parameters (i.e., pressure, temperature, water/steam mass-flow rates), in the various WHR plant components, were thermodynamically optimized in order to maximize the DF–WHR CP efficiency (η_{CP}), defined as:

$$\eta_{CP} = \frac{P_{DFE} + P_{ST} - P_{MFP} - P_{SCP}}{M_f LHV_f} \quad (8)$$

where P_{DFE} is the DF engine power; P_{ST} the steam turbine power; P_{MFP} and P_{SCP} the main feed and steam condenser pump powers; and M_f and LHV_f the fuel mass-flow rate and the lower heating value, respectively.

The WHR steam-plant optimization procedure starts from the definition of a series of fixed parameters, reported in Table 3, referring to the DF engine operating at NCR conditions, fueled by NG, and assuming a vertical configuration for the HRSG.

Table 3. Fixed parameters of WHR system referring to DF engine operating at 75 % of MCR load.

Fixed WHR Plant Parameters	NG Fuel
Engine exhaust gas mass flow rate (kg/s)	26
Engine exhaust gas temperature (°C)	352
Condenser pressure (bar)	0.08
Plan dimensions of the HRSG (m × m)	1.85 × 2.10

Once the fixed parameters in Table 3 were defined, the WHR steam plants were optimized by varying the HRSG optimization parameters reported in Table 4, with the aim of maximizing the η_{CP} parameter (Equation (8)). The efficiency of the DF-WHR combined plant η_{CP} is in fact the objective function to be optimized in the optimization process concerning the HRSG parameters shown in Table 4.

Table 4. Variation range and variation steps of HRSG optimization parameters.

HRSG Optimization Parameters	Variation Range	Variation Steps
HRSG steam drum pressure (bar)	5–20	0.1
Pinch point temp. differences: ΔT_{pp} (°C)	5–20	1
Approach point temperature diff.: ΔT_{ap} (°C) for superheated steam plant	5–35	1

The main results of the optimization procedure carried out for the WHR steam plants combined with the DF engine are shown in the following Tables 5 and 6 relative to the DF engine powered by NG or HFO, respectively. In both Tables the percentage differences reported in the fourth column were calculated as follows:

$$\Delta x/x\% = \frac{x_{SH\ SP} - x_{S\ SP}}{x_{S\ SP}} 100[\%] \quad (9)$$

where x represents the considered parameter and suffixes SH SP and S SP indicate the superheated- and saturated-steam plant, respectively.

Table 5. Optimization of WHR steam plants combined with DF engine powered by NG.

Optimized HRSG Parameters	NG Fuel		
	WHR Saturated Steam	WHR Superheated Steam	WHR Difference (%)
HRSG steam drum pressure (bar)	7.6	8	5.26
Pinch point temp. difference: ΔT_{pp} (°C)	5.1	5	−1.96
Approach point temp difference: ΔT_{ap} (°C)	-	17	-
Optimized Main HRSG Data			
HRSG height [m]	4.33	5.04	16.26
HRSG weight [t]	28.75	33.26	15.67
Economizer pipe number	7	6	−14.29
Evaporator pipe number	34	34	0.0
Superheater pipe number	-	7	-

The obtained optimization results in case of the engine powered by NG are reported in the second and third columns of Table 5 for saturated and superheated steam, respectively, while percentage differences are shown in the fourth column. The upper and lower part of the table refer to the thermodynamic and constructive parameters of the HRSG, respectively.

Table 6. Main HRSG data and WHR plant data in DF engine powered by Heavy Fuel Oil (HFO).

HRSG Parameters	HFO Fuel		
	WHR Saturated Steam	WHR Superheated Steam	WHR Difference (%)
HRSG steam drum pressure (bar)	7.1	7.3	2.81
Pinch point temp. difference: ΔT_{pp} (°C)	7.2	7.9	9.72
Approach point temp difference: ΔT_{ap} (°C)	-	7.3	-
WHR Plants Data			
ST inlet pressure (% of p_{SD})	70	70	0.0
HRSG gas outlet temperature (°C)	165.3	169.3	2.38

Table 6 shows the HRSG parameters in the case of the DF engine powered by HFO, running at NCR, obtained taking into account the temperature and mass-flow rates of the exhaust gases generated by this fuel (see Figure 1). In this case, the geometrical data of the HRSG components were the same, determined by the optimization procedure relative to the engine powered by NG (see Table 5).

Similar to the case of Table 5, the data reported in the second and third column of Table 6 refer to saturated- and superheated-steam WHR plants, respectively. In order to satisfy the already mentioned constraint of steam pressure for ship steam services (at least 7 bar of HRSG SD pressure), it is necessary to partially close the Isenthalpic Lamination Valve (ILV in WHR plant schemes of Figures 2 and 3) to reduce pressure in the steam turbine inlet section to 70% of SD pressure, as reported in Table 6.

Table 6 shows that, for the engine running at NCR, both WHR plants satisfied the constraint that gas temperature at the HRSG outlet should remain over the 160 °C limit, as required by the engine manufacturers when HFO is used as fuel due to the sulfur present in it, which causes acid corrosion at lower temperatures. The same temperature limit was also satisfied in the other considered engine loads.

7. WHR Steam-Plants Comparison

A first comparison between saturated-steam (Figure 2) and superheated-steam (Figure 3) WHR plants is shown in the fourth column of Tables 5 and 6, referring to NG and HFO engine fuel, respectively. The comparison data reported below are relative to the engine running at NCR load conditions.

Percentage differences relative to optimized HRSG parameters, reported in the fourth column of Table 5 (NG fuel), showed small difference (5.26%) for HRSG SD pressure, and even smaller difference (−1.96%) for pinch point temperature difference (ΔT_{pp}).

Differences of the same parameters were 2.81% and 9.72% in the case of HFO fuel (fourth column of Table 6), respectively. Greater difference was observed for main optimized HRSG data, shown in the fourth column of Table 5, regarding HRSG height and weight (both about 16%).

Figure 4 shows details of saturated- and superheated-steam HRSG plants in terms of height (Figure 4a) and weight (Figure 4b) for HRSG components (economizer, evaporator, superheater, and shell).

No considerable differences could be found between saturated- and superheated-steam plants with regard to the weight, height, and number of pipes (see Table 5) of the economizers and evaporators. Figure 4 shows that the greater height and weight of the superheated-steam plant was mainly due to the superheater. Figure 4a shows the considerable shell contribution in overall HRSG height, while its contribution in total HRSG weight was small, as reported in Figure 4b.

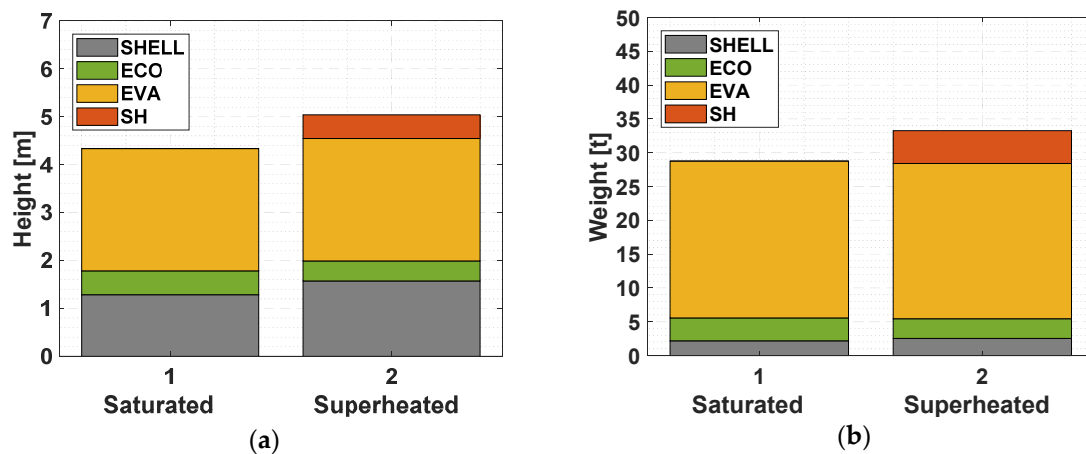


Figure 4. (a) Height and (b) weight of saturated- and superheated-steam HRSG plant components.

7.1. WHR Steam Plants Performance in Design Working Conditions

Considerations similar to those expressed in the comment of Figure 4 can be drawn from the more detailed HRSG data reported in Table 7.

Analysis of the most important data reported in Table 7 led to the following considerations:

Below are the formulas used to calculate the efficiency of the HRSG and its heat exchangers. With reference to Figures 2 and 3 and to the captions of Figures 2 and 3, these formulas are:

$$\text{HRSG}_{\text{eff}} = \frac{T_{1g} - T_{4g}}{T_{1g} - T_{\text{amb}}} 100 [\%] \quad (10)$$

$$\text{EV}_{\text{eff}} = \frac{(T_{2g} - T_{3g})}{(T_{2g} - T_{2s})} 100 [\%] \quad (11)$$

$$\text{E}_{\text{eff}} = \frac{(T_{3g} - T_{4g})}{(T_{3g} - T_{00\text{SC}})} 100 [\%] \quad (12)$$

$$\text{SH}_{\text{eff}} = \frac{(T_{1g} - T_{2g})}{(T_{1g} - T_{3\text{sd}})} 100 [\%] \quad (13)$$

From these formulas, we understand how EV efficiency was higher than that of E and the SH, as is easy to deduce from Figures 6 and 7.

Despite less superheater efficiency (12.43% for NG and 6.14% for HFO, line 17 in Table 7), the exchanged superheater thermal power (line 14) reduced the evaporators' exchanged thermal powers by about 15% for NG and 10% for HFO (line 10), being practically equal the evaporator efficiency in the saturated- and superheated-steam plants (line 13).

In the superheated-steam plant, when compared to the saturated one, the less exchanged evaporator thermal power (about 15% (NG) and 10% (HFO)) involved similar (about 15% and 10%, respectively) economizer water-mass flow-rate reduction (line 5 in Table 7), able to maintain about the same steam drum pressure between the saturated and superheated plants, as reported in Table 5 (NG) and Table 6 (HFO). Similar less economizer efficiency (line 9 in Table 7) in the superheated plant, compared to the saturated one, was observed for both NG and HFO engine fuels. Greater HRSG gas-side pressure loss (more than 16% for both considered engine fuels) was observed in the superheated plant compared to the saturated one (line 3 of Table 7); that, however, did not substantially reduce engine efficiency.

Table 7. Saturated- and superheated-steam HRSG parameters and percentage differences in engines powered by NG or HFO.

HRSG Parameters	NG Fuel			HFO Fuel		
	WHR Sat. Steam	WHR Superh. Steam	WHR Diff. (%) $\Delta x/x$ 100	WHR Sat. Steam	WHR Superh. Steam	WHR Diff. (%) $\Delta x/x$ 100
1 Overall HRSG _{eff} (%)	58.37	56.85	−2.61	48.40	46.95	−2.99
2 HRSG gas outlet temperature (°C)	160.3	165.2	3.08	165.3	169.3	2.38
3 HRSG gas side pressure loss (mbar)	30.01	34.94	16.46	43.03	50.27	16.52
4 Exchanged E thermal power (MW)	0.36	0.32	−10.66	0.26	0.24	−7.15
5 E water-mass flow rate (kg/s)	2.27	1.91	−15.85	2.44	2.18	−10.65
6 E water inlet temperature (°C)	121.1	125.3	3.47	134.2	136.8	1.94
7 E water outlet temperature (°C)	157.8	161.7	2.47	165.2	166.1	0.54
8 E gas inlet temperature (°C)	174.1	177.8	2.16	173.4	176.8	2.00
9 E efficiency (%)	26.26	21.87	−16.72	20.96	18.03	−13.94
10 EV exchanged thermal power (MW)	4.77	4.04	−15.35	4.06	3.64	−10.18
11 EV steam drum temperature (°C)	168.3	170.4	1.24	165.6	166.7	0.66
12 EV gas inlet temperature (°C)	350	328	−6.29	297.0	287.6	−3.17
13 EV efficiency (%)	97.19	96.46	−0.75	94.46	93.80	−0.71
14 SH exchanged thermal power (MW)	-	0.62	-	-	0.27	-
15 SH steam outlet temperature (°C)	-	332.9	-	-	289.7	-
16 SH gas inlet temperature (°C)	-	350.0	-	-	297.0	-
17 SH efficiency (%)	-	12.43	-	-	6.14	-

The saturated- and superheated-steam plants were characterized by very similar overall efficiency, as reported in line 1 ($HRSG_{eff}$) of Table 7, with an advantage of near 10% in the case of NG fuel compared to HFO fuel. The same considerations can be deduced from Figure 5, where available HRSG gas thermal power is also reported in the third column.

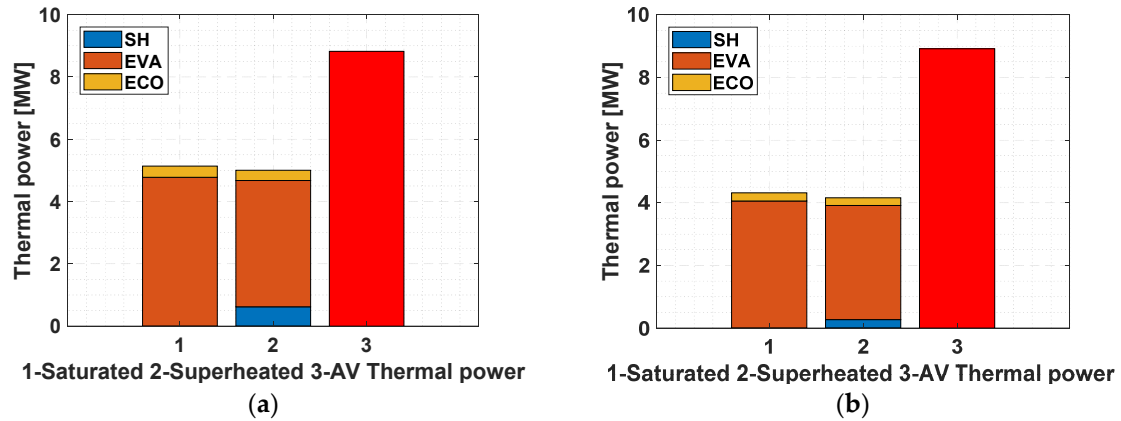


Figure 5. Engine exhaust gas thermal power (3) and thermal power recovered by (1) saturated- and (2) superheated-steam plant heat exchangers: E, EV, and SH, with an engine powered by (a) NG or (b) HFO.

Figure 6 shows the temperature profiles of gas and water/steam flows along the HRSG versus waste heat recovery for the saturated-steam plant with an engine fed by (a) NG or (b) HFO. The same is shown in Figure 7 for the superheated-steam plant.

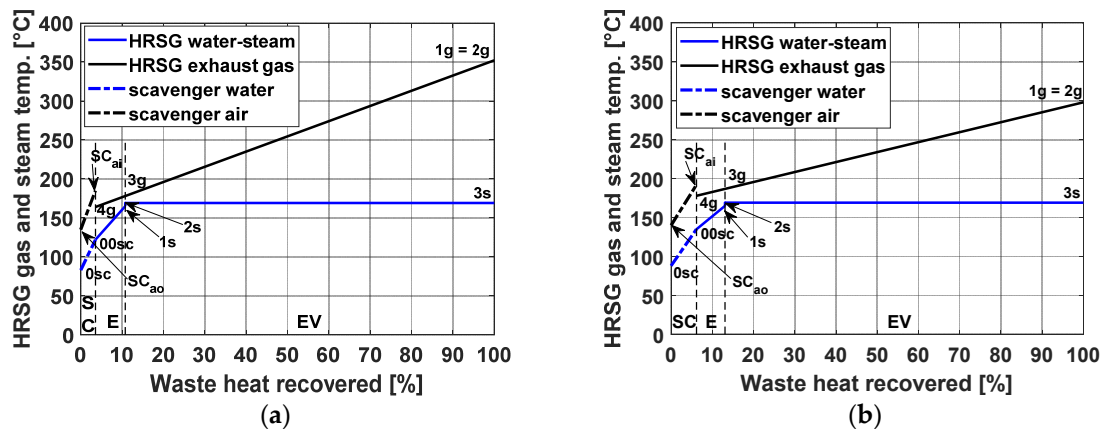


Figure 6. Temperature profiles along HRSG for saturated-steam plant with an engine powered by (a) NG or (b) HFO.

Further information on the engine, steam plants, and the DF engine–WHR combined system can be found in Table 8. Line 1 of Table 8 shows that, with the engine powered by NG, HRSG back pressure for both types of steam plant increased the engine-specific fuel consumption by only about 1 g, and by slightly more with the engine powered by HFO. With both types of fuel, engine efficiency remained substantially the same for the saturated- and the superheated-steam plant (line 2 in Table 8). Line 3 of Table 8 shows that Rankine cycle efficiency was very similar in the cases of the engine powered by NG or HFO; a greater cycle efficiency of 6.91% was observed in the case of NG fuel for the superheated-steam plant compared to the saturated-steam one, and this difference dropped to 4.41% when using HFO.

Table 8. Engine, steam-plant components, and DF engine–WHR combined plants: main data and percentage differences in engine powered by NG or HFO.

Engine, Steam-Plant Components, and Combined Plant Data		NG Fuel			HFO Fuel		
		WHR Sat. Steam	WHR Superh. Steam	WHR Diff. (%) $\Delta x/x$ 100	WHR Sat. Steam	WHR Superh. Steam	WHR Diff. (%) $\Delta x/x$ 100
1	HRSG p loss. E_{sfc} incr. (g/kWh)	0.92	1.07	16.46	1.31	1.52	16.50
2	η_E (%)	47.28	47.23	−0.10	45.67	45.61	−0.12
3	$\eta_{Rankine}$ (%)	26.16	27.96	6.91	25.80	26.91	4.41
4	η_{CP} (%)	50.88	51	0.25	47.93	47.95	0.05
5	NCR engine power (kW)	13162.5	13162.5	0.0	13162.5	13162.5	0.0
6	ST power (kW)	1014.0	1062.5	4.81	657.2	679.6	3.41
7	ST inlet pressure (% of p_{SD})	100	100	0.0	70	70	0.0
8	ST ΔH_{id} (kJ/kg)	678.2	825.7	21.76	494.1	570.4	15.43
9	ST mass flow rate (kg/s)	2.10	1.74	−17.38	1.87	1.61	−13.90
10	ST efficiency (%)	71.0	74.0	4.18	71.2	74.0	3.89
11	ST outlet steam quality	0.87	0.97	12.00	0.87	0.95	9.40
12	condenser thermal power (kW)	4390	4074.6	−7.18	3918.7	3591.1	−5.81
13	SCP pump power (kW)	17.63	16.32	−7.46	11.63	10.98	−5.57
14	MFP pump power (kW)	4.51	4.99	10.8	3.58	4.16	16.24
15	SSS mass flow rate (kg/s)	0.17	0.17	0.0	0.57	0.57	0.0

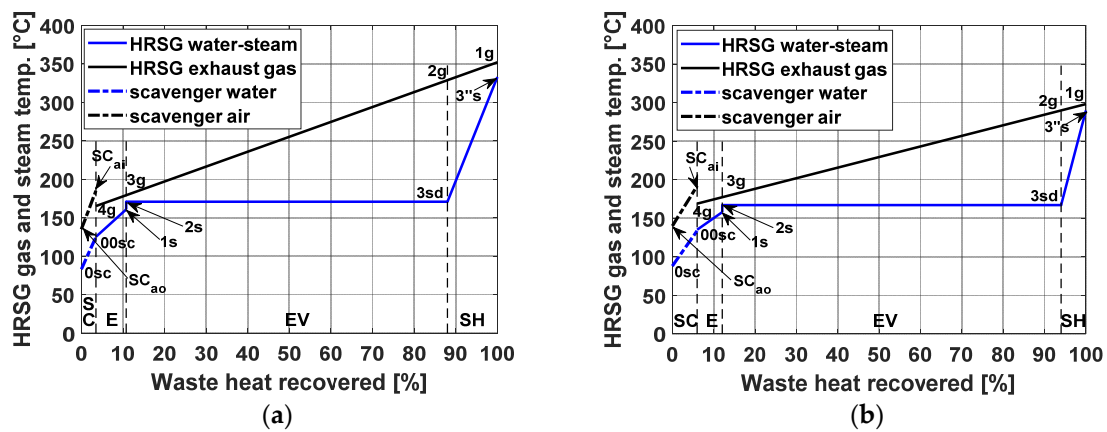


Figure 7. Temperature profiles along HRSG for superheated-steam plant with an engine powered by (a) NG or (b) HFO.

Line 4 of Table 8 shows about the same DF engine–WHR combined plant efficiency (η_{CP}), determined by Equation (8), in the case of NG fuel. A similar result was observed in the case of HFO fuel, although with a difference of about 3% in favor of NG. The slight ST power difference between the saturated- and superheated-steam plants that occurred with both tested fuel types, as shown in line 6 of Table 8, was due to a greater ST enthalpy drop in the case of the superheated-steam plant (line 8); that, however, was approximately compensated by greater ST mass-flow rate (line 9) in the case of the saturated-steam plant.

Table 8 shows that ST power with the engine powered by HFO was about 35% lower than that with the engine powered by NG. This is mainly due to less ST enthalpy drop (line 8) in the case of HFO fuel, motivated by the need to partially close the ILV valve (Table 6) to maintain SD pressure at 7 bar at least, as required by ship steam services. In the case of the engine powered by HFO, greater steam-mass-flow rate was also required by ship steam services (line 15 of Table 8) compared to the case of the engine powered by NG, contributing to a decrease of ST mass-flow rate, and therefore, of its power. ST efficiencies were similar (line 10 in Table 8) with a little advantage for the superheated-steam plant due to greater steam quality at the ST outlet (line 11). The powers of the SCP and MFP pumps, much lower than the ST power (about 0.8% and 0.2%, respectively), as shown in lines 6, 13, and 14 of Table 8, had practically no influence on efficiency η_{CP} of the DF engine–WHR combined plant (see Equation (8)).

7.2. WHR Steam-Plants Performance in Off-Design Working Conditions

In this section, we compare the DF engine–WHR combined plants in the cases of an engine powered by NG or HFO, as well as for different engine loads: 50%, 75% (adopted for WHR plant-component design optimization), 85%, and 100% of the engine MCR. Figure 8 and the following show the different parameters that define the DF engine and the components of the WHR steam plants, highlighting the percentage differences between the parameters of the superheated- and the saturated-steam plant. These percentage differences, calculated with Equation (9), are displayed for the different engine loads mentioned. In the figures, the horizontal lines signed with 0 represent zero-percent difference values.

As shown in Figure 8a,b, pertinent to NG and HFO fuel, respectively, the delivered engine power (DF Engine_{br}) was always maintained constant regardless of the used WHR plant. With regard to the Steam Condensed Pump and the Main Feed Pump (SCP and MFP in the schemes of Figures 2 and 3), the power differences between the two compared WHR plants and types of fuel generally increased as engine load decreased, especially in the case of the MFP pump (Figure 8a). However, these differences had negligible influence on the engine–WHR combined plant efficiency (Equation (8)), as their power was much lower than ST power.

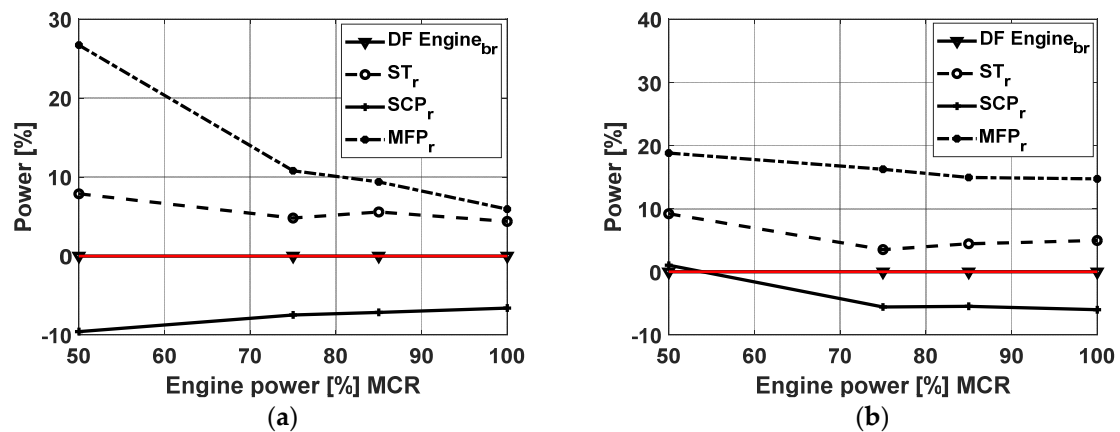


Figure 8. Engine and WHR plant components: power versus engine load with an engine powered by (a) NG or (b) HFO.

The same figure shows a little advantage (always less than 10%) of real delivered ST power (ST_r) of the WHR superheated-steam plant, for all considered engine powers and fuel types. This small power difference could be explained by individual analysis of ST parameters, reported in Figure 9.

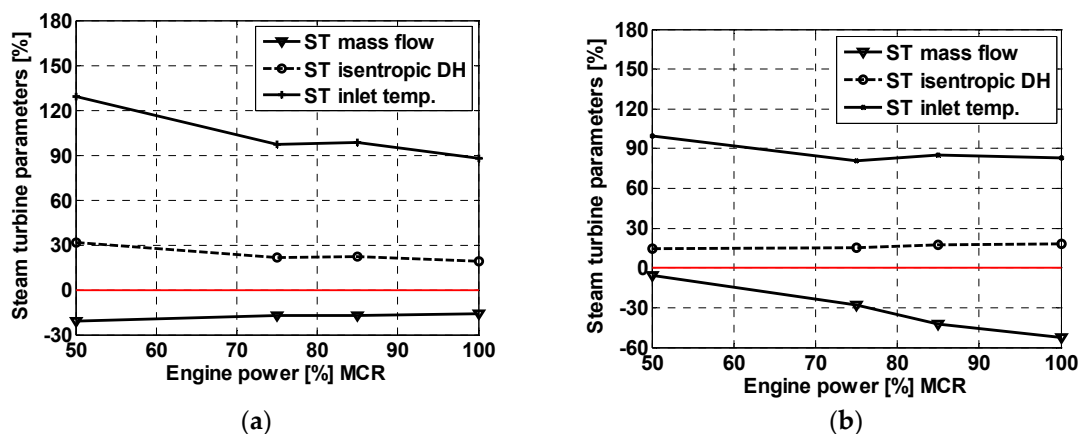


Figure 9. Steam-turbine parameters versus engine load with an engine powered by (a) NG or (b) HFO.

Indeed, from Figure 9a, pertinent to NG fuel, a greater ST isentropic-enthalpy percentage drop (DH) can be observed in the superheated cycle, as opposed to an approximately equal smaller percentage mass flow. This substantial equivalence between the ST isentropic-enthalpy percentage drop increase and the mass flow percentage decrease is due to superheater presence in the HRSG, that reduces the gas temperature entering the evaporator; it follows that to obtain the desired steam drum pressure (very similar for saturated and superheated steam plants), the processed water-steam flow rate must be reduced, compared to the case of the saturated steam plant, in which the gas temperature at the evaporator inlet is the same as at the outlet of the engine turbocharger.

This ST parameter compensation was less evident in the case of HFO fuel (Figure 9b), as is indicated by the ST power variation in Figure 8b.

Figure 10a,b shows a comparison of the saturated- and superheated-steam WHR plants in terms of HRSG efficiency as a whole and of its components, particularly the evaporator and economizer, also including the temperature of the exhaust gas at the HRSG outlet (T_{4g} in plant schemes of Figures 2 and 3).

As can be seen from the figure, overall HRSG efficiency in the case of the superheated-steam plant was lower than that obtained in the case of the saturated-steam plant for all considered engine loads, with the exception of the 50% engine load in the case of HFO engine fuel (Figure 10b). This is due to very similar evaporator efficiency between the two compared steam plants and fuel types, and greater

difference (about 18% with NG fuel, less in the HFO case) regarding economizer efficiency in favor of the saturated-steam plant.

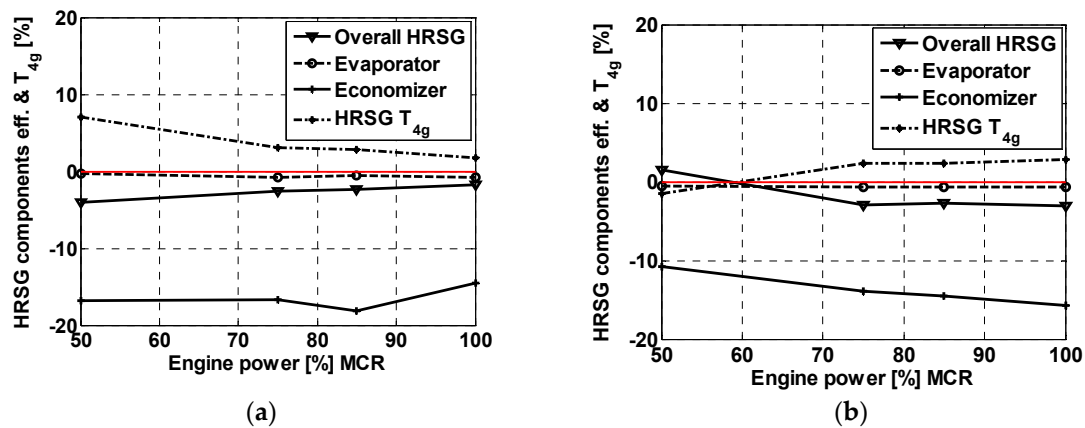


Figure 10. HRSG and components efficiency comparison versus engine load with an engine powered by (a) NG or (b) HFO.

This last effect on overall HRSG efficiency was mitigated by the much lower exchange of thermal power of the economizer compared to that of the evaporator. The HRSG exhaust gas temperature difference (HRSG T_{4g} in Figure 9a) was always positive (greater value in superheated-steam WHR plant) and increased slightly as engine load decreased.

In the case of HFO engine fuel (Figure 10b), this parameter difference was slightly negative only at 50% engine load. This was probably due to the ILV valve being partially closed for the reasons already mentioned.

Data reported in Figure 11a,b regarding the efficiency comparison of engine, combined WHR plants and their components showed less efficiency of the saturated Rankine cycle compared to the superheated one. This difference increased as engine load decreased in the case of NG fuel (Figure 11a), while it increased with an engine load in the case of HFO fuel, as shown in Figure 11b, probably due to the partial closing of the ILV valve when engine load decreased. Steam-turbine efficiency was also about 4% greater in the superheated-steam plant for all engine loads in the case of NG fuel (Figure 11a); when engine fuel was HFO, it remained constant at 4% for high engine loads, and increased from 4% to 6% only for a 50% MCR engine load.

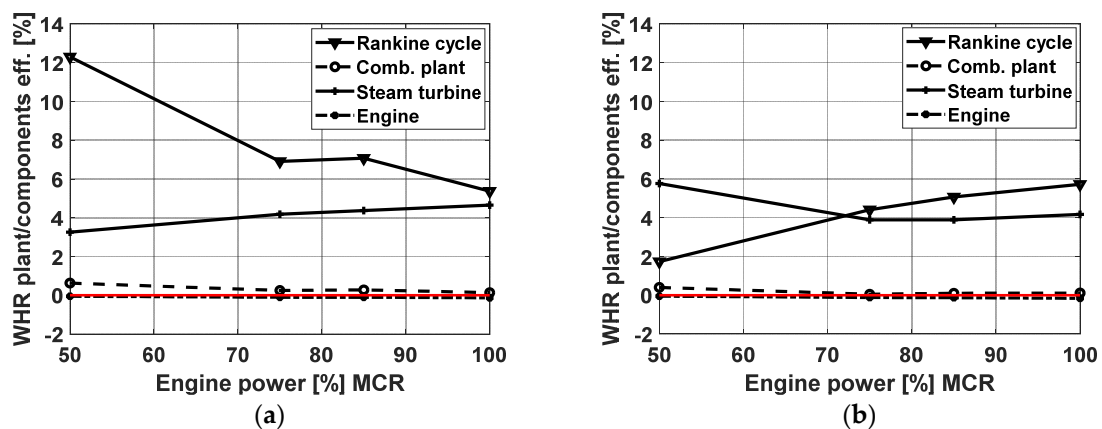


Figure 11. WHR plant and component-efficiency comparison versus engine load with an engine using (a) NG or (b) HFO.

Despite this, the difference of the combined plant efficiencies was always very small (with an advantage for the superheated-steam plant mainly in the case of NG fuel). This was due to greater

engine power value compared to steam-turbine power, as reported in lines 5 and 6 of Table 8 for the NCR engine load. In fact, from Table 8 it can be estimated that the ST power is less than 8% of the engine power in case of NG fuel, and about 5% of the engine power in case of HFO.

8. Exergetic Analysis

In the preceding sections, we made a comparison between the two WHR in light of the first principle of thermodynamics. More complete analysis should also consider the second principle, taking into account the irreversibility of the real processes, accompanied by entropy production corresponding to energy loss.

In other words, the energy-recovery process should be evaluated not only from a quantitative but also from a qualitative point of view. To this aim, a useful approach is represented by exergetic analysis. The exergy of a system at a certain thermodynamic state may be defined as “the maximum amount of work that can be obtained when the system moves from that particular state to a state of equilibrium with the surroundings” [32].

For a thermomechanical process with stationary flow, specific exergy Ex can be calculated as follows:

$$Ex = (h - h_0) - T_0 (s - s_0) \quad (14)$$

where h and s are the specific enthalpy and entropy, and subscript 0 refers to ambient conditions.

In our study, it was of particular interest to evaluate, for the considered process, the exergy efficiency, commonly defined as:

$$\eta_{ex} = \frac{\text{Useful Exergy from the process}}{\text{Total Exergy to the process}} = \frac{W_{real}}{H_{ef}} \quad (15)$$

where W_{real} is the real work obtained by the process and H_{ef} is the exergy heat amount delivered to the process by the fuel.

It is possible to rewrite the previous equation on the basis of the first principle of thermodynamics:

$$\eta_{ex} = \frac{W_{real}}{Q_{in} \left(1 - \frac{T_0}{T}\right)} = \frac{W_{real}/Q_{in}}{\left(1 - \frac{T_0}{T}\right)} \quad (16)$$

In the last term of the preceding equation, the numerator represents energy efficiency η_{en} (ratio between real work and incoming heat Q_{in}), while the denominator is Carnot efficiency η_c . Thus, it is possible to write [32,33]:

$$\eta_{ex} = \frac{\eta_{en}}{\eta_c} \quad (17)$$

The above-described formulation was applied to evaluate the considered WHR systems from an exergetic point of view as well. The involved thermodynamic processes are characterized by the following main input data, differing according to the selected type of WHR plant, the type of fuel used, and the engine-load conditions:

- engine exhaust gas temperature (T in Equation (16));
- cooling-water temperature at condenser inlet (depending on the ambient conditions); and
- Rankine cycle efficiency (η_{en} in Equation (17)).

The most important results of the developed analysis are shown in the following figures.

Using HFO as engine fuel, Figure 12a shows that exergetic efficiency tendentially increased with decreasing engine power for both the saturated- and the superheated-steam plant. The variation of Rankine cycle efficiency was different with decreasing engine power. As shown in Figure 12b, a slight decrease of efficiency with decreasing engine power from 100% to 75% was followed by an increase when engine load decreased from 75% to 50%.

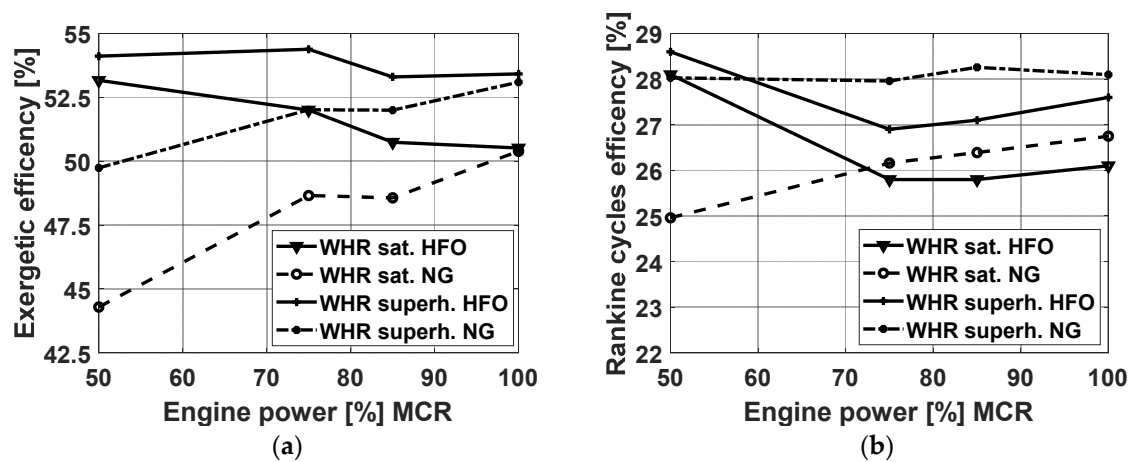


Figure 12. WHR steam-plant (a) exergetic and (b) energetic efficiency variations versus engine power.

The tendential increase of exergetic efficiency with decreasing engine load from 100% to 75% can be explained by considering that the efficiencies of both Rankine and Carnot cycle decreased at the same time (see Figure 1a).

The situation that occurred when using NG as engine fuel was quite different. In this case, Rankine cycle efficiency, as shown in Figure 12b, remained almost constant when varying engine load, while Carnot efficiency tended to increase with the decrease of engine load (see Figure 1a). This explains the reduction of exergetic efficiency with the decrease of engine load, more marked in the case of the saturated-steam plant, when using NG as engine fuel.

9. Conclusions

Using available simulation models, it was possible to carry out a detailed comparison between the considered saturated- and superheated-steam WHR plants, applied to the waste-heat recovery of the same DF marine engine. The comparison evidenced substantial equivalence between them with regards to the efficiency of the DF engine–WHR combined plants in all considered engine powers for the engine fueled by NG or HFO. A 3% higher efficiency is observed in the case of the engine powered by NG at normal continuous rating.

The reasons of this substantial overall performance equivalence between single-pressure saturated- and superheated-steam WHR plants, with an advantage for the NG engine fuel, were analyzed in this paper in detail and were about the same for the two considered engine-fuel types. These reasons can be summarized in the substantial equivalence of the HRSG efficiency, with an advantage of about 10% in favor of the NG-fueled engine running at NCR, and in minor differences regarding the power of the steam turbine (never higher than 9%), always related to the same engine-fuel type.

With regard to HRSG height and weight, the saturated-steam plant was characterized by a reduction of about 16% compared to the superheated-steam plant.

The lower steam quality at the turbine outlet for the saturated-steam plant, compared to the superheated one, about equal for both engine fuels, was a disadvantage for the saturated-steam plant, because of the lower turbine efficiency and the greater damage of the turbine blades, both due to higher steam humidity in the saturated-steam cycles. To reduce erosion of turbine blades, determined by steam humidity, turbine manufacturers usually use more resistant blade materials to keep ST maintenance-time intervals about equal between saturated- and superheated-steam cycles.

With regard to the overall costs of the considered WHR steam plants based on a saturated- or superheated-steam cycle, it can be said as a first approximation that they were approximately equal, the greater cost of the superheater in the HRSG in some way being compensated by the greater cost of the steam turbine operating with the saturated-steam cycle, because of the better material used for the

turbine blades. However, these economic aspects would require more in-depth analysis and could be developed in the near future.

The authors believe that the research carried out and the obtained results may represent a contribution in the direction of increasing the efficiency of marine propulsion systems based on the use of dual-fuel (diesel fuel and natural gas) engines, characterized by a series of technical and environmental advantages. They also believe that the availability of suitable simulation procedures could be applied to optimize and compare the different solutions currently used or that are under development for the propulsion of commercial LNG carriers.

Author Contributions: The authors are part of a research group where two departments of the University of Genoa and one department of the University of Naples have collaborated on topics of common interest. Although the tasks entrusted to the individual participants have been appropriately differentiated (bibliographic research, development and validation of computational codes, comparison of results, writing of the article, subsequent revisions of it, etc.), it can be stated the substantial equivalence of the contribution that each author has provided, in quantitative and qualitative terms, for the preparation of this article. All authors have read and agreed to the published version of the manuscript.

Funding: This research received no external funding.

Acknowledgments: The authors would like to express their deepest gratitude to Alessandro Sabattini of Fincantieri S.p.A. and MAN Diesel and Turbo for supporting the present research. Particular thanks are due to Andrea Rossetto of Ranieri Tonissi S.p.A. Genova.

Conflicts of Interest: The authors declare no conflict of interest.

Abbreviations List

AC	Aftercooler
B.m.e.p.	Brake mean effective pressure
C	Turbocharger compressor
DF	Dual fuel
Diff	Difference
E	Economizer
EG	Electric generator
EV	Evaporator
HFO	Heavy fuel oil
HRSG	Heat recovery steam generator
HWT	Heat water tank
ILV	Isenthalpic lamination valve
JW	Jacket water
MCR	Maximum continuous rating
MDO	Marine diesel oil
MFP	Main feed pump
NCR	Normal continuous rating
NG	Natural gas
Sat	Saturated steam
SC	Scavenging system
SCO	steam condenser
SCP	Steam condenser pump
SD	Steam drum
ST	Steam turbine
Superh	Superheated steam
T	Turbocharger turbine, temperature
WHR	Waste heat recovery

References

1. Le Fevre, C.N. *A Review of Demand Prospects for LNG as a Marine Fuel*; Oxford Institute for Energy Studies: Oxford, UK, 2018; ISBN 978-1-78467-114-3.
2. International Maritime Organization (IMO). *Report of the Marine Environment Protection Committee (MEPC) on its Fifty-Seventh Session*; IMO: London, UK, 2008.
3. Marine Environment Protection Committee (MEPC). Resolution, MECP 212 (63/23), Annex 8. Adopted on 2 March 2012. Guidelines to the Method of Calculation of the Attained Energy Efficiency Design Index (EEDI) for New Ships. Available online: <http://www.imo.org/en/KnowledgeCentre/IndexofIMOResolutions/Marine-Environment-Protection-Committee-%28MEPC%29/Documents/MEPC.212%2863%29.pdf> (accessed on 22 December 2019).
4. Marine Environment Protection Committee (MECP). In Proceedings of the International Maritime Organization (IMO), 66th Session, London, UK, 31 March–4 April 2014.
5. Altosole, M.; Benvenuto, G.; Campora, U.; Laviola, M.; Zaccone, R. Simulation and Performance Comparison between Diesel and Natural Gas Engines for Marine Applications. *Proc. Inst. Mech. Eng. Part M J. Eng. Marit. Environ.* **2017**, *231*, 690–704. [[CrossRef](#)]
6. Livanos, G.A.; Theotokatos, G.; Pagonis, D.N. Techno-economic investigation of alternative propulsion plants for Ferries and RoRo ships. *Energy Convers. Manag.* **2014**, *79*, 640–651. [[CrossRef](#)]
7. Serrano, J.R.; Olmeda, P.; Tiseira, A.; García-Cuevas, L.M.; Lefebvre, A. Theoretical and experimental study of mechanical losses in automotive turbochargers. *Energy* **2013**, *55*, 888–898. [[CrossRef](#)]
8. Altosole, M.; Benvenuto, G.; Campora, U.; Silvestro, F.; Terlizzi, G. Efficiency Improvement of a Natural Gas Marine Engine Using a Hybrid Turbocharger. *Energies* **2018**, *11*, 1924. [[CrossRef](#)]
9. Mamat, A.M.; Romagnoli, A.; Martinez-Botas, R.F. Characterisation of a low pressure turbine for turbocompounding applications in a heavily downsized mild-hybrid gasoline engine. *Energy* **2014**, *64*, 3–16. [[CrossRef](#)]
10. Poran, A.; Thawko, A.; Eyal, A.; Tartakovsky, L. Direct injection internal combustion engine with high-pressure thermochemical recuperation-Experimental study of the first prototype. *Int. J. Hydrog. Energy* **2018**, *43*, 11969–11980. [[CrossRef](#)]
11. Choi, Y.; Negash, A.; Kim, T.Y. Waste heat recovery of diesel engine using porous medium-assisted thermoelectric generator equipped with customized thermoelectric modules. *Energy Convers. Manag.* **2019**, *197*. [[CrossRef](#)]
12. Javani, N.; Dincer, I.; Naterer, G.F. Thermodynamic analysis of waste heat recovery for cooling systems in hybrid and electric vehicles. *Energy* **2012**, *46*, 109–116. [[CrossRef](#)]
13. Altosole, M.; Benvenuto, G.; Campora, U.; Laviola, M.; Trucco, A. Waste Heat Recovery from Marine Gas Turbines and Diesel Engines. *Energies* **2017**, *10*, 718. [[CrossRef](#)]
14. Tu, H.; Fan, H.; Lei, W.; Zhou, G. *Options and Evaluations on Propulsion Systems of LNG Carriers*; IntechOpen©: London, UK, 2019. [[CrossRef](#)]
15. Fernández, I.A.; Gómez, M.R.; Gómez, J.R.; Insua, Á.B. Review of propulsion systems on LNG carriers. *Renew. Sustain. Energy Rev.* **2017**, *67*, 1395–1411. [[CrossRef](#)]
16. Ioannidis, J. *Thermo Efficiency System (TES) for Reduction of Fuel Consumption and CO₂ Emission*; Aalborg A.G.: Copenhagen, Denmark, 1984.
17. Hansen, J.P. Diesel engine waste Heat Recovery-Possibilities and Limitations. In Proceedings of the ICMES 90, Maritime Systems Integrity, the University of Newcastle-upon-Tyne, Great Britain, UK, 19–21 September 1990.
18. Schmid, H. *Less Emissions through Waste Heat Recovery*; Wartsila Switzerland Ltd.: Winterthur, Switzerland, 2004.
19. Tien, W.K.; Yeh, R.H.; Hong, J.M. Theoretical Analysis of Cogeneration System for Ships. *Energy Convers. Manag.* **2007**, *48*, 1965–1974. [[CrossRef](#)]
20. Dzida, M.; Muchasrki, J. On the Possible Increasing of Efficiency of Ship Power Plant with the System Combined of marine Diesel Engine, Gas Turbine and Steam Turbine, at the Main Engine-Steam Turbine Mode of Cooperation. *Polish Marit. Res.* **2009**, *16*, 47–52. [[CrossRef](#)]
21. Grimmeliuss, H.; Boonen, E.J.; Nicolai, H.; Stapersma, D. The integration of Mean Value First Principle Diesel Engine models in Dynamic Waste Heat and Cooling Load Analysis. In Proceedings of the CIMAC Congress, Bergen, Norway, 14–17 June 2010; p. 280.

22. Dimopoulos, G.G.; Georgopoulou, C.A.; Kakalis, N.M.P. Modelling and Optimisation of an Integrated Marine Combined Cycle System. In Proceedings of the ECOS 2011, Novi Sad, Serbia, 4–11 July 2011; pp. 1283–1298.
23. MAN Diesel & Turbo. *Waste Heat Recovery System (WHRS) for Reduction of Fuel Consumption, Emissions and EEDI*; MAN Diesel & Turbo Society: Copenhagen, Denmark, 2011.
24. Benvenuto, G.; Campora, U.; Trucco, A. Optimization of Waste Heat Recovery from the Exhaust Gas of Marine Diesel Engines. *Proc. Inst. Mech. Eng. Part M J. Eng. Marit. Environ.* **2014**, *230*, 83–94. [[CrossRef](#)]
25. Zymaris, A.S.; Alnes, Ø.Å.; Knutsen, K.E.; Kakalis, N.M.P. Towards a model-based condition assessment of complex marine machinery systems using systems engineering. *Energy Res.* **2016**, *10*, 75–85. [[CrossRef](#)]
26. Altosole, M.; Campora, U.; Laviola, M.; Zaccone, R. Waste Heat Recovery from Dual-Fuel Marine Engine. In *Maritime Transportation and Harvesting of Sea Resources*; Soares, C.G., Teixeira, À.P., Eds.; Taylor and Francis Group: London, UK, 2018; ISBN 978-0-8153-7993-5.
27. Altosole, M.; Campora, U.; Laviola, M.; Zaccone, R. Deterioration effects on the performance of a steam plant for the waste heat recovery from a marine diesel engine. *Ships Offshore Struct.* **2019**. [[CrossRef](#)]
28. Andreasen, J.G.; Meroni, A.; Haglind, F. A Comparison of Organic and Steam Rankine Cycle Power Systems for Waste Heat Recovery on Large Ships. *Energies* **2017**, *10*, 547. [[CrossRef](#)]
29. Benvenuto, G.; Campora, U.; Laviola, M.; Zaccone, R. Comparison of Waste Heat Recovery Systems for the Refitting of a Cruise Ferry. In Proceedings of the NAV 2015, 18th International Conference on Ships and Shipping Research, Lecco, Italy, 24–26 June 2015; Altosole, M., Francescutto, A., Eds.; pp. 404–415, ISBN 978-88-940557-1-9.
30. MAN Diesel & Turbo. *MAN 51/60DF Project Guide, Marine Four Stroke Dual Fuel Engine*; MAN Diesel & Turbo: Copenhagen, Denmark, 2014.
31. Cohen, H.; Rogers, G.F.C.; Saravanamuttoo, H.I.H. *Gas Turbine Theory*, 3rd ed.; Longman Scientific and Technical: Harlow, Essex, UK, 1987.
32. Gundersen, T. An introduction to the concept of exergy and energy quality. *Energy Process Eng.* **2011**, *4*, 1–26.
33. Baldi, F.; Gabrielli, C. A feasibility analysis of waste heat recovery systems for marine applications. *Energy* **2015**, *80*, 654–665. [[CrossRef](#)]



© 2020 by the authors. Licensee MDPI, Basel, Switzerland. This article is an open access article distributed under the terms and conditions of the Creative Commons Attribution (CC BY) license (<http://creativecommons.org/licenses/by/4.0/>).